Journal of Solid State Chemistry 184 (2011) 2623–2628

Contents lists available at ScienceDirect

Journal of Solid State Chemistry

journal homepage: www.elsevier.com/locate/jssc

Mild hydrothermal synthesis, crystal structure, thermal behaviour, spectroscopic and magnetic properties of $(NH_4)_{0.80}Li_{0.20}[Fe(AsO_4)F]$

Teresa Berrocal [a], José L. Mesa [b], Edurne S. Larrea [a], Begoña Bazán [a], José L. Pizarro [a], Luis Lezama [b], Teófilo Rojo [b], María I. Arriortua [a,*]

[a] Departamento de Mineralogía y Petrología, Facultad de Ciencia y Tecnología, Universidad del País Vasco, UPV/EHU, Apdo. 644, 48080 Bilbao, Spain
[b] Departamento de Química Inorgánica, Facultad de Ciencia y Tecnología, Universidad del País Vasco, UPV/EHU, Apdo. 644, 48080 Bilbao, Spain

ARTICLE INFO

Article history:
Received 27 June 2011
Received in revised form
26 July 2011
Accepted 28 July 2011
Available online 3 August 2011

Keywords:
Hydrothermal synthesis
Crystal structure
Thermal analysis
Spectroscopy
Magnetism

ABSTRACT

The $(NH_4)_{0.80}Li_{0.20}[Fe(AsO_4)F]$ compound has been synthesized under mild hydrothermal conditions. The compound crystallize in the orthorhombic $Pna2_1$ space group, with cell parameters $a=13.352(9)$, $b=6.7049(9)$, $c=10.943(2)$ Å and $Z=8$. The compound belongs to the $KTiO(PO_4)$ structure type, with chains alternating FeO_4F_2 octahedra and AsO_4 tetrahedra, respectively, running along the "*a*" and "*b*" crystallographic axes. The diffuse reflectance spectrum in the visible region shows the forbidden electronic transitions characteristic of the Fe(III) d^5-high spin cation in slightly distorted octahedral geometry. The Mössbauer spectrum at room temperature is characteristic of iron (III) cations. The ESR spectra, carried out from room temperature to 200 K, remain isotropic with variation in temperature; the *g*-value being 1.99(1). Magnetic measurements indicate the predominance of strong antiferromagnetic interactions.

1. Introduction

The research on phosphates, phosphites and arsenates compounds with new open frameworks is currently in progress due to their potential applications in catalysis, gas separation or as ion exchangers [1,2]. Among the many open-framework compounds known, those based on the phosphate oxoanion appear to be the predominant class [1,3,4]. In addition to the use of tetrahedral phosphate groups as building units, other anionic moieties such as borates [5], arsenates [6], sulphates [7] and selenates [8] have been used successfully in the preparation of novel open framework structures. Of these, the arsenates are interesting because, although arsenic belongs to the same group as phosphorous, the larger size of the AsO_4^{3-} anion can give rise to different structures and/or physical properties. Thus, many arsenate frameworks of different structure and composition has been prepared and characterized [6,9–15]. Besides, the addition of fluoride anions into the reaction mixture, developed by Kessler and Ferey and co-workers [16], has led to the discovery of new microporous structural types, some of them exhibiting very large channels such as in cloverite [17], ULM-5 [18], MIL-31 [19], MIL-46 [20] and VSB-5 [21]. In these phases, the fluorine anions are part of the coordination sphere of the metal cation. A systematic study of the fluorine systems [16b] has shown that the geometry of the structure-directing agent plays an important role for the attainment of three-dimensional open framework. It has also been observed that the ammonium groups from the organic molecules preferentially interact with the fluorine atoms of the framework via hydrogen bonds.

In the last years, to establish relationships between the templates and the inorganic framework, the scientist working in this research field have focused their attention on nitrogen rich molecules, such as ethylenediamine, 1,3-diaminopropane, piperazine, 1,4-diazabicyclo[2.2.2]octane, 1,4,8,11-teraazacyclotetradecane, etc. [22]. In these organically templated compounds the crystal structure collapses after losing the organic cation under heating. However, precursor materials with an open framework containing small particles, such as the ammonium cations, inside the inorganic skeleton, could provide a new synthetic route to obtain new condensed phases by thermal treatment of the appropriate kind of precursors. Furthermore, the use of both the ammonium cation and the fluoride anion together with an appropriate synthetic procedure could favour the attainment of new porous materials after thermal treatment of the resulting precursor. In this way, recently, we have synthesized the new orthorhombic, Imam, $Fe(AsO_4)$ phase that exhibits a condensed structure with textural porosity [23]. This arsenate has been prepared as single-crystals by heating single-crystals of the $(NH_4)[Fe(AsO_4)F]$ precursor, which allows the elimination of $(NH_4)F$. However, the $(NH_4)[Fe(PO_4)F]$ phosphate [24] does not exhibit this kind of thermal behaviour.

* Corresponding author. Fax: +34 946 013 500.
E-mail address: maribel.arriortua@ehu.es (M.I. Arriortua).

0022-4596/$ - see front matter © 2011 Elsevier Inc. All rights reserved.
doi:10.1016/j.jssc.2011.07.043

In this work we report on the mild hydrothermal synthesis of the $(NH_4)_{0.80}Li_{0.20}[Fe(AsO_4)F]$ compound with $KTiO(PO_4)$-type structure [25]. The thermal, spectroscopic and magnetic properties of this phase are also reported and discussed in this work, on basis of its crystal structure.

2. Experimental section

2.1. Synthesis and characterization

The $(NH_4)_{0.80}Li_{0.20}[Fe(AsO_4)F]$ compound was synthesized hydrothermally under autogeneous pressure, at 170 °C for five days. The starting reagents were $Fe_2(SO_4)_3 \cdot 7H_2O$ (0.37 mmol), $As_2O_5 \cdot 3H_2O$ (3.69 mmol), $Li(OH) \cdot H_2O$ (0.28 mmol), NH_4OH (1 mL, 28 wt%) and HF (1 mL, 48 wt%) in approximately 30 mL of water with an initial pH near to 6. The reaction mixture was stirred to visual homogeneity and then sealed in a PTFE-lined stainless steel pressure vessel (fill factor 60%). After reaction, slow cooling to room temperature at approximately 30 K h^{-1} was carried out. No appreciable change in the solution pH was observed. The product consists of well-formed light-green single crystals. The composition of this phase was analyzed by inductively coupled plasma atomic emission spectroscopy (ICP-AES) and C, N, H-elemental analysis. The fluorine content was obtained using a fluoride selective electrode. Found: Fe, 24.3(2); As, 32.6(1); N, 2.8(2); H, 0.6(1); F, 8.2(3); Li, 0.6(2) for $(NH_4)_{0.80}Li_{0.20}[Fe(AsO_4)F]$ and requires: Fe, 24.6; As, 33.1; N, 3.0; H, 0.9; F, 8.4; Li, 0.7. The density was measured by flotation method, using a mixture of diiodomethane (CH_2I_2, $\rho = 3.32$ g cm^{-3}) and chloroform (Cl_3CH, $\rho = 1.49$ g cm^{-3}). The value obtained for $(NH_4)_{0.80}Li_{0.20}[Fe(AsO_4)F]$ was 3.09(2) g cm^{-3}.

2.2. Single-crystal X-ray diffraction study

A prismatic single-crystal was carefully selected under a polarizing microscope and mounted on a glass fibre. Single-crystal X-ray diffraction data were collected at room temperature on an Oxford Diffraction Xcalibur2 automatic diffractometer (Mo-$K\alpha$ radiation) equipped with a CCD detector. The data reduction procedure and absorption corrections were carried out using the diffractometer software [26], and performed taking into account the size and shape of the crystal. The structure was solved and refined using the SHELX 97 program [27]. The hydrogen atoms of the ammonium ion are delocalized around the nitrogen atom, so it could not be possible to assign their position. On the other hand, lithium ions could not be localized because the amount of this element in the structure is very low, there are only 0.2 lithium atoms per formula. Anisotropic thermal parameters were assigned to all atoms. Details of crystal data, intensity collection, and some features of the structural refinement are reported in Table 1. The crystal structure can be solved in either the acentric *Pna*21 or the centric *Pnam* space group. When the refinement is performed in the acentric space group the ammonium cations are placed in two different crystallographic positions. However, if the centric space group is used the ammonium cations must be considered as disordered with occupancy factors of 50%, maintaining the pseudoinversion centre of the inorganic skeleton The value of 0.52(2) obtained for the Flack parameter in the refinement of the structure was a clear indication for a racemic twinning in the crystal studied. Consequently, the final refinement was performed including a correction for twinning by inversion, obtaining values of $R_1 = 0.0241$ and BASF = 0.522 [23]. Finally, a simulation based on the single-crystal structure was in excellent agreement with the X-ray powder diffraction data, indicating the presence of pure phases with high crystallinity. Further details on the crystal structure may be obtained from the ICSD upon quoting the depository number 423133. All the structure drawings were performed using the ATOMS program [28].

2.3. Physicochemical characterization techniques

The analytical measurements were carried out using ICP-AES Perkin Elmer 4110 ZL spectrometer. A SDC 2960 Simultaneous DSC-TGA TA Instrument, under a flow of air with heating rate of 5 °C min^{-1}, was used to perform the thermogravimetric analysis up to 800 °C. The calibration in mass was carried out using a standard with known mass; the calibration in temperature was performed with In, Zn, Al and Ag. The DSC calibration was made using a sample of sapphire. Time resolved X-ray thermodiffractometry was carried out in air atmosphere on a PHILIPS X'PERT automatic diffractometer (Cu$K\alpha$ radiation) equipped with a variable-temperature stage (Anton Paar HTK16) and a Pt sample holder. The powder patterns were recorded in 2θ steps of 0.02° in the range $5 \leq 2\theta \leq 50$, counting for 2 s per step and recording the diagrams every 15 °C from room temperature up to 795 °C. IR

Table 1
Crystal data, structure resolution and refinement for $(NH_4)_{0.80}Li_{0.20}[Fe(AsO_4)F]$.

Empirical formula	$FeAsO_4N_{0.8}H_{3.25}Li_{0.2}F$
Formula weight	229.29
Crystal system, space group (No.)	Orthorhombic, $Pna2_1(33)$
Unit cell dimensions	$a = 13.352(2)$ Å, $b = 6.7049(9)$ Å, $c = 10.943(2)$ Å
Volume, Z	979.6(3) $Å^3$, 8
$\rho_{obs.}$, $\rho_{calc.}$	3.09(2), 3.11 g/cm^3
F(000)	874
Temperature	293(2) K
Absorption coefficient, μ	9.725 mm^{-1}
Wavelength, λ(Mo $K\alpha$)	0.71073 Å
Crystal size	0.13 × 0.13 × 0.15 mm
θ range	3.05–29.81°
Limiting indices	$-15 \leq h \leq 17$, $-9 \leq k \leq 9$, $-14 \leq l \leq 12$
Reflections collected/unique	7992/2370
R(int)	0.03
Data/restraints/parameters	2370/1/146
Final R indices [$I > 2\sigma(I)$]	$R_1 = 0.0241$, $wR_2 = 0.0588$
R indices (all data)	$R_1 = 0.0265$, $wR_2 = 0.0596$
Completeness to $\theta = 29.81$	92.4%
$w = 1/[\sigma^2\|F_o\|^2 + (xp)^2]$, $p = [\max\|F_o\|^2 + 2\|F_c\|^2]/3$	$x = 0.066$
Largest diff. peak and hole	0.578 and −0.743 e $Å^{-3}$
Goodness-of-fit on F^2	1.124

spectrum (KBr pellet) was collected using a Nicolet FT-IR 740 spectrophotometer in the spectral range 4000–400 cm^{-1}. Electrochemical impedance spectroscopy (EIS) measurements were conducted using a Solartron 1260 impedance analyzer. The frequency range was 10^{-2}–10^{6} Hz with signal amplitude of 300 mV. All of these electrochemical experiments were performed over polycrystalline sample at equilibrium from 260 °C to 30 °C, under zero dc current intensity and under air over a cycle of heating and cooling, with a cooling rate of 20 °C/h. The sample was compacted by a uniaxial press and the tablet was placed between the electrodes, using as current collectors platinum mesh. Between 260 and 220 °C the semicircles were observed, not being well defined in any case. Below this temperature only a dispersion of points was observed (see Figs. 1 and 2 of Supplementary material). The conductivity values obtained from the fittings of the spectra are very low (on the order of magnitude of 10^{-9}), so the compound can be considered as an insulator. Mössbauer spectra were obtained using a constant-acceleration Mössbauer spectrometer with a ^{57}Co/Rh source. Velocity calibration was done using a metallic Fe foil, and the Mössbauer spectral parameters are given relative to this standard at room temperature. The Mössbauer spectra were fitted with the NORMOS program [29]. Diffuse reflectance spectrum was registered at room temperature on a Varian Cary 5000 spectrometer in the spectral range 2000–210 nm, using a white Teflon to record the baseline. A Bruker ESP 300 spectrometer, operating at X band, was used to record the ESR polycrystalline spectra between 20 and 300 K. The magnetic field was measured with a Bruker BNM 200 Gaussmeter and the frequency inside the cavity was determined using a Hewlett-Packard 5352B microwave frequency counter. Magnetic measurements on powdered sample were performed in the temperature range 5.0–300 K, using a Quantum Design MPMS-7 SQUID magnetometer. The applied magnetic field was 0.1 T, a value in the range of linear dependence of magnetization vs. magnetic field, even at 5.0 K.

3. Results and discussion

3.1. Crystal structure

The structural framework of the title compound is $KTiO(PO_4)$-type [30]. Selected bond distances and angles are given in Table 2. The structure can be described as a three-dimensional framework constructed from corner-sharing (FeO_4F_2) octahedra and (AsO_4) tetrahedra. Chains formed by alternating ($Fe(1)O_4F_2$) or ($Fe(2)O_4F_2$) octahedra and ($As(1)O_4$) or ($As(2)O_4$) tetrahedra, respectively, are running along the [100] and [010] directions, and are linked by common oxygen vertices (Fig. 1). The chains are interconnected through the fluorine atoms belonging to the (FeO_4F_2) octahedra. This architecture forms channels of six polyhedra running along the *a*- and *b*-axes in which the Li^+ and $(NH_4)^+$ are located. The Li^+ and $(NH_4)^+$ groups compensate for the anionic charge of the $[Fe(AsO_4)F]^-$ inorganic skeleton. Each crystallographic nitrogen atom is surrounded by nine possible H-bond acceptors, with distances N–O, F ranging from 2.829(7) to 3.282(7) Å for N(1) and from 2.760(6) to 3.458(8) Å for N(2) (See Table 1 of Supplementary

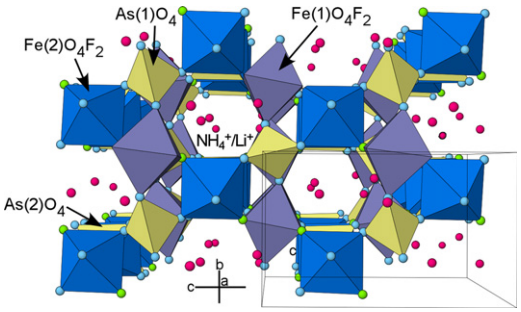

Fig. 1. Polyhedral view of the KTP-type crystal structure of $(NH_4)_{0.80}Li_{0.20}[Fe(AsO_4)F]$.

Table 2
Bond lengths (Å) and angles (deg.) for $(NH_4)_{0.80}Li_{0.20}[Fe(AsO_4)F]$.

As(1)O$_4$ tetrahedra					
As(1)–O(8)^{i}	1.693(3)	O(8)^{i}–As(1)–O(1)^{ii}	112.0(2)	O(1)^{ii}–As(1)–O(3)	109.3(2)
As(1)–O(1)^{ii}	1.697(5)	O(8)^{i}–As(1)–O(7)	109.7(2)	O(7)–As(1)–O(3)	111.1(2)
As(1)–O(7)	1.708(5)	O(1)^{ii}–As(1)–O(7)	104.2(1)	O(8)^{i}–As(1)–O(3)	110.4(1)
As(1)–O(3)	1.713(3)				
As(2)O$_4$ tetrahedra					
As(2)–O(2)	1.687(3)	O(2)–As(2)–O(6)	110.0(1)	O(2)–As(2)–O(5)	110.5(2)
As(2)–O(6)	1.689(3)	O(2)–As(2)–O(4)	111.9(2)	O(6)-As(2)–O(5)	107.4(3)
As(2)–O(4)	1.691(5)	O(6)–As(2)–O(4)	110.5(2)	O(4)–As(2)–O(5)	106.3(2)
As(2)–O(5)	1.701(5)				
Fe(1)O$_4$F$_2$ octahedra					
Fe(1)–O(5)	1.931(5)	O(5)–Fe(1)–O(4)^{iii}	91.9(1)	O(8)–Fe(1)–F(2)	90.5(2)
Fe(1)–O(4)^{iii}	1.965(4)	O(5)–Fe(1)–O(8)	90.5(2)	F(1)–Fe(1)–F(2)	86.6(1)
Fe(1)–O(8)	2.000(3)	O(4)^{iii}–Fe(1)–O(8)	93.6(2)	O(5)–Fe(1)–O(3)	90.4(2)
Fe(1)–F(1)	2.005(4)	O(5)–Fe(1)–F(1)	91.6(2)	O(4)^{iii}–Fe(1)–O(3)	84.7(2)
Fe(1)–F(2)	2.026(4)	O(4)^{iii}–Fe(1)–F(1)	172.5(2)	O(8)–Fe(1)–O(3)	178.0(2)
Fe(1)–O(3)	2.068(3)	O(8)–Fe(1)–F(1)	93.0(2)	F(1)–Fe(1)–O(3)	88.7(2)
		O(5)–Fe(1)–F(2)	177.9(2)	F(2)–Fe(1)–O(3)	88.7(2)
		O(4)^{iii}–Fe(1)–F(2)	89.8(2)		
Fe(2)O$_4$F$_2$ octahedra					
Fe(2)–O(1)	1.974(5)	O(1)–Fe(2)–F(2)^{iv}	91.5(3)	O(7)–Fe(2)–F(1)	88.8(3)
Fe(2)–F(2)^{iv}	1.987(4)	O(1)–Fe(2)–O(7)	177.8(3)	O(2)–Fe(2)–F(1)	94.6(2)
Fe(2)–O(7)	1.991(5)	F(2)^{iv}–Fe(2)–O(7)	89.4(2)	O(1)–Fe(2)–O(6)^{v}	88.6(2)
Fe(2)–O(2)	2.019(3)	O(1)–Fe(2)–O(2)	92.1(2)	F(2)^{iv}–Fe(2)–O(6)^{v}	91.4(2)
Fe(2)–F(1)	2.025(4)	F(2)^{iv}–Fe(2)–O(2)	88.2(2)	O(7)–Fe(2)–O(6)^{v}	89.3(2)
Fe(2)–O(6)^{v}	2.047(3)	O(7)–Fe(2)–O(2)	90.0(2)	O(2)–Fe(2)–O(6)^{v}	179.2(2)
		O(1)–Fe(2)–F(1)	90.3(2)	F(1)–Fe(2)–O(6)^{v}	85.7(2)
		F(2)^{iv}–Fe(2)–F(1)	176.6(3)		

Symmetry codes: i=$x,y+1,z$; ii=$-x+1/2,y+1/2,z+1/2$; iii=$-x,-y,z+1/2$; iv=$-x+1/2,y+1/2,z-1/2$; v=$x+1/2,-y+1/2,z$.

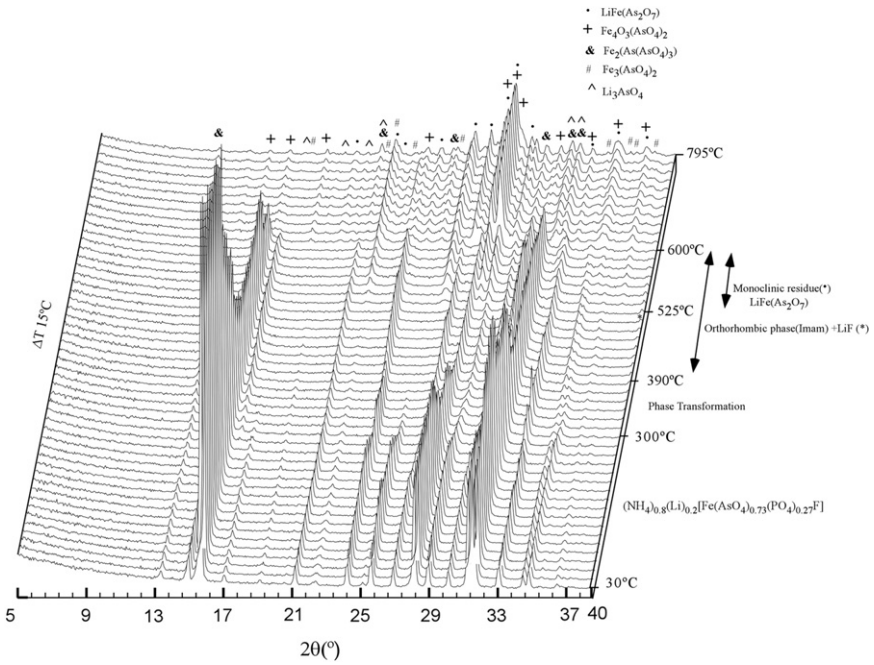

Fig. 2. Thermodiffractograms of $(NH_4)_{0.80}Li_{0.20}[Fe(AsO_4)F]$.

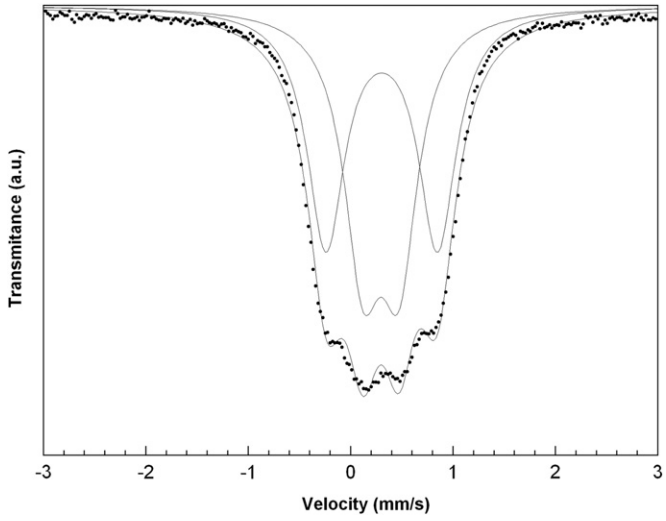

Fig. 3. Mössbauer spectrum for $(NH_4)_{0.80}Li_{0.20}[Fe(AsO_4)F]$.

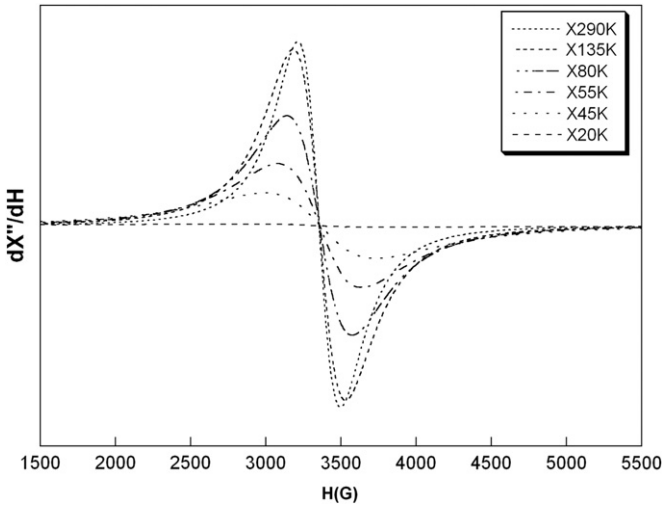

Fig. 4. Powder X-band ESR spectrum of $(NH_4)_{0.80}Li_{0.20}[Fe(AsO_4)F]$.

material), consequently it is possible that the ammonium cations are disposed in different orientations hindering the location of the hydrogen atoms.

In both octahedra, the iron(III) cations are linked to the oxygen atoms belonging to the (AsO_4) tetrahedra with a mean Fe–O, F bond distance of 2.00(4) Å . The hexacoordination is completed with two fluoride ions bonded at a mean bond distance of 2.01(2) Å. The fluorine ions are in *cis* in the ($Fe(1)O_4F_2$) octahedra and in *trans* in the ($Fe(2)O_4F_2$). The *cis*- and *trans*-O, F–Fe–O, F bond angles range between 94.6(1)° and 84.7(2)° and 179.2(1)° and 172.5(2)°, respectively, as expected for slightly distorted octahedral geometry around the Fe(III) cations. The arsenic atoms are in tetrahedral coordination with an average As–O bond distance of 1.70(1) Å, and O–As–O angles near 109(2)°, as expected in the arsenate compounds with a sp^3 hybridization. The distortion of the ($Fe(1)O_4F_2$) and ($Fe(2)O_4F_2$) octahedra and $As(1)O_4$ and ($As(2)O_4$) tetrahedra from that of an ideal octahedron and tetrahedron, evaluated by the Alvarez et al. [31]method, is S(Oh)=0.117, 0.069 and S(Td)=0.086, 0.045, respectively, for each polyhedron.

3.2. Thermal behaviour

The TG curve shows an exothermic mass loss of 16% between 280 and 500 °C, which corresponds to the loss of the ammonium and fluoride ions. Above 500 °C, the TG curve continues decreasing with two endothermic peaks, probably due to the decomposition of the arsenate groups and the formation of the inorganic residue. This residue was analyzed by powder X-ray diffraction, being a mixture of five phases: $LiFe(As_2O_7)$ phase [32a], $Fe_4O_3(AsO_4)_2$ [32b]; $Fe_2(As(AsO_4)_3)$ [32c]; $Fe_3(AsO_4)_2$ [32d] and $Li_3(AsO_4)$ [32e].

Thermal behaviour was also studied using time-resolved X-ray thermodiffractometry in air. The diffractograms (Fig. 2) indicate that the thermal stability limit is 300 °C. Above 390 °C, the phase is transformed into a mixture of the Imam orthorhombic $Fe(AsO_4)$

[23] and the cubic LiF phase [32f]. In the 525–600 °C temperature range the Imam $Fe(AsO_4)$ exists together with the $LiFe(As_2O_7)$ phase [32a]. Above 600 °C, and up to the end of the heating process, the crystallization of rest of the mixture of residues obtained in the thermogravimetric analysis takes place.

3.3. IR, Mössbauer and UV–vis spectroscopies

The IR spectrum shows a strong band at 3200 cm^{-1} that corresponds to the stretching vibrational mode of the $(NH_4)^+$ cation. The bending mode of this cation is observed near to 1470 cm^{-1}. The IR spectrum also shows the characteristic vibrational modes of the arsenate oxoanion at typical frequencies [33]. The anti-symmetric stretching mode, ν_{as}(As–O), appears at approximately 810 cm^{-1}. The symmetric stretching mode, ν_s(As–O), is observed at approximately 730 cm^{-1}. Finally, the anti-symmetric deformation vibration, δ_{as} (O–As–O) is detected at 520 and 470 cm^{-1}.

The Mössbauer spectrum performed at room temperature shows two doublets belonging to the two different crystallographic positions of the Fe(III) cations (Fig. 3). The values of the isomer shift and the quadrupolar splitting are 0.4007(1), 1.0891(1) mm s^{-1} for Fe(1) and 0.4144(1), 0.3531(5) mm s^{-1} for Fe(2). The relation between the integrated areas of these signals is approximately 1:1, in good agreement with the multiplicity of the two general crystallographic positions occupied by the Fe(III) cations.

The diffuse reflectance spectrum shows four bands at the frequencies: ν_1, 13,240; ν_2, 18,020; ν_3, 22,890 and ν_4, 25,380 cm^{-1}. The intensity of all these bands is weak, as expected for the spin forbidden transitions between the ground state, $^6A_{1g}(^6S)$ and the excited levels $^4T_{1g}(^4G)$; $^4T_{2g}(^4G)$; $^4A_{1g}$, $^4E_g(^4G)$ and $^4T_{2g}(^4D)$ of the Fe(III) d^5 high-spin cation, in regular octahedral symmetry [34]. The Dq and Racah (B and C) parameters were calculated using the Tanabe–Sugano energy expressions [35]. The values obtained were 1150 cm^{-1} for Dq and 785 and 3020 cm^{-1} for B and C, respectively. These values are in the range habitually found for the Fe(III) cation in slightly distorted octahedral environment. The reduction of the B-parameter value with respect to that of the free Fe(III) (1150 cm^{-1}) is approximately 30%, suggesting an appreciable covalent character in the Fe–O, F chemical bonds.

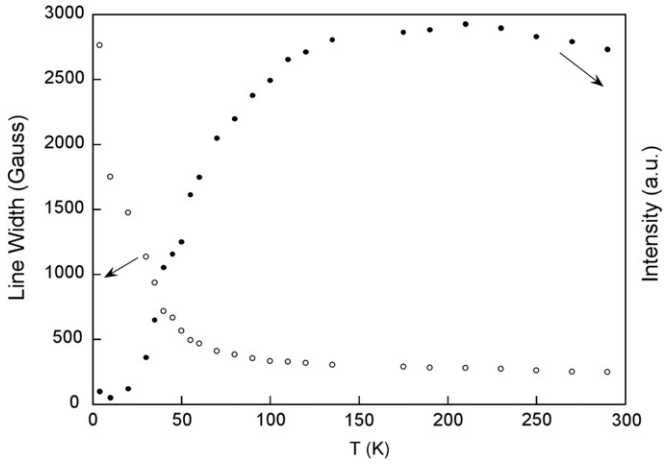

Fig. 5. Temperature dependence of the intensity of the ESR signals and the line width for $(NH_4)_{0.80}Li_{0.20}[Fe(AsO_4)F]$.

3.4. Magnetic behaviour

3.4.1. ESR measurements

The ESR spectrum was recorded on powder sample at X-band between 20 and 290 K (Fig. 4). The isotropic signal is centred at a magnetic field of 3350 G, remaining, practically, constant upon cooling the sample in all the temperature range studied. The *g*-value, with a value of 1.99, remains unchanged with the variation of temperature. This *g*-value is characteristic of octahedrally coordinated d^5-high spin Fe(III) cation.

The thermal variation of the intensity and the line-width of the signals, calculated by fitting the experimental spectra to Lorentzian curves, are displayed in Fig. 5. The intensity of the signal increases with decreasing temperature from room temperature to 150 K, whereas, below 100 K, a decrease of the signal is shown. This result can be associated with the existence of strong antiferromagnetic interactions in the compound. The line-width of the ESR signals increases from room temperature down to approximately 50 K, as a consequence of the dipolar homogeneous broadening [36]. When the temperature is further decreased, the line-width increases vigorously. This fact is due to a strong spin correlation [36].

3.4.2. Magnetic measurements

Magnetic measurements were carried out on powdered sample from room temperature to 5.0 K (Fig. 6). The measurements

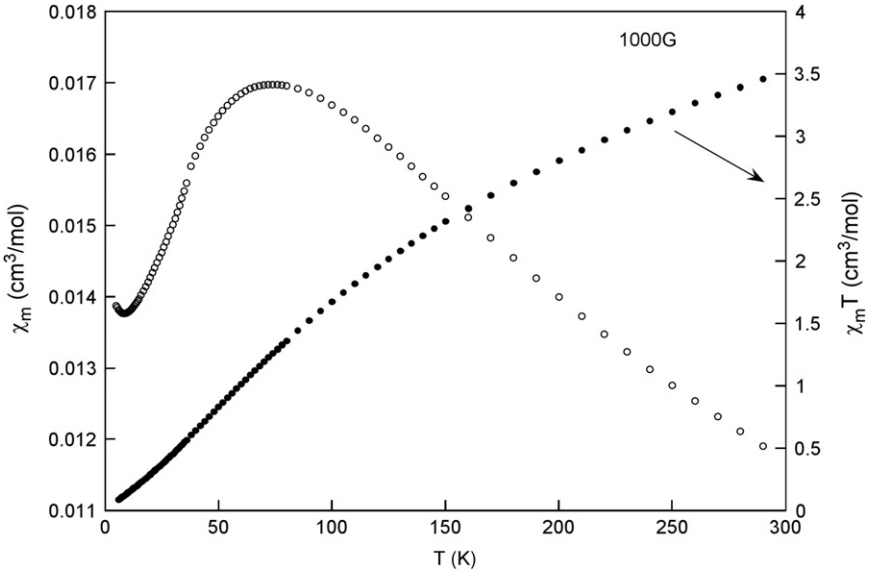

Fig. 6. Thermal evolution of the χ_m and $\chi_m T$ curves of the $(NH_4)_{0.80}Li_{0.20}[Fe(AsO_4)F]$ phase.

performed at 1000 G in the zero field cooling (ZFC) and field cooling (FC) modes show reversibility. The molar magnetic susceptibility, χ_m, increases with decreasing temperature down to 80 K, temperature at which the magnetic susceptibility shows a broad maximum. After this temperature the susceptibility shows a strong decrease down to 8 K. Finally, the susceptibility increases again, suggesting the existence of a paramagnetic impurity. This impurity must be in a very little proportion, as is shown by the small value of $\chi_m T$ product at low temperatures. The thermal evolution of $1/\chi_m$ was fitted to a Curie–Weiss law over 150 K, but the values obtained for the Curie constant and the Weiss temperature (7.12 cm^3K/mol and -449 K) were not the expected for an iron(III) compound. The continuous decrease observed in the $\chi_m T$ product from 3.48 to 0.04 $cm^3\,K\,mol^{-1}$, suggests that $(NH_4)_{0.80}Li_{0.20}[Fe(AsO_4)F]$ has an antiferromagnetic character.

The structure of the $(NH_4)_{0.80}Li_{0.20}[Fe(AsO_4)F]$ phase is built up from perpendicular chains where the metal centres are linked through fluorine ions with angles near 133°. This value favours the antiferromagnetic interactions. Trials to fit the thermal evolution of the molar susceptibility with a classical chain model and with a model taking into account the interchain contacts [37] were carried out without much success. This fact suggests that the magnetic interaction model of the phase is more complex and cannot be described with the classical models.

4. Concluding remarks

The $(NH_4)_{0.80}Li_{0.20}[Fe(AsO_4)F]$ compound has been synthesized by mild hydrothermal technique. The compound exhibits a three-dimensional structure, constructed from two perpendicular chains along the "*a*" and "*b*" axes. The thermal stability limit is 390 °C. The Dq and Racah parameters have values of 1150 cm^{-1} and 785, 3020 cm^{-1}, respectively. The Mössbauer spectrum indicates the existence of two doublets belonging to the two different crystallographic positions of the Fe(III) cations. The ESR spectrum is isotropic with a *g*-value of 1.99, characteristic of octahedrally coordinated d^5-high spin Fe(III) cation. Magnetic measurements indicate the existence of a global antiferromagnetic ordering.

Acknowledgments

This work has been financially supported by the "Ministerio de Ciencia e Innovación, MICINN" (MAT-2010-15375) and the "Consejería de Educación, Universidades e Investigación—Gobierno Vasco" (IT-177.07). We wish to thank the technicians of SGIker (UPV/EHU), Drs. J. Sangüesa, I. Orue, A. Larrañaga, J.C. Raposo and P. Vitoria, financed by the National Program for the Promotion of Human Resources within the National Plan of Scientific Research, Development and Innovation (MICINN) and the European Social Found (ESF). Edurne S. Larrea thanks the "Dirección de Política Científica - Gobierno Vasco," for her postdoctoral contract.

Appendix A. Supporting information

Supplementary data associated with this article can be found in the online version at doi:10.1016/j.jssc.2011.07.043.

References

[1] A.K. Cheetham, G. Férey, T. Loiseau, Angew. Chem. Int. Ed. 38 (1999) 3268–3292.
[2] M.E. Davis, Chem. Eur. J. 3 (11) (1997) 1745–1750.
[3] P.B. Moore, in: J. Niagru, P.B. Moore (Eds.), Crystallochemical Aspects of the Phosphate Minerals, Springer-Verlag, Berlin, 1984.
[4] (a) S. Feng, R. Xu, Acc. Chem. Res. 34 (2001) 239–247;
(b) J. Yu, R. Xu, Acc. Chem. Res. 36 (2003) 481–490.
[5] I.D. Williams, M. Wu, H.H.-Y. Sung, X.X. Zang, J. Yu, Chem. Commun. (1998) 2463–2464.
[6] J.S. Chen, L. Li, G.D. Yang, R.R. Xu, J. Chem. Soc., Chem. Commun. (1989) 1217–1218.
[7] C.N.R. Rao, E.V. Sampathkumaran, R. Natarajan, G. Paul, J.N. Behera, A. Choudhury, Chem. Mater. 16 (2004) 1441–1446 and references therein.
[8] J.N. Behera, A.A. Ayi, C.N.R. Rao, Chem. Commun. (2004) 968–969 and the references therein.
[9] R.C. Haushalter, Z. Wang, L.M. Meyer, S.S. Dhingra, M.E. Thompson, J. Zubieta, Chem. Mater. 6 (1994) 1463–1464.
[10] S.-L. Wang, Y.-H. Lee, Inorg. Chem. 33 (1994) 3845–3847.
[11] F. Gagnard, C. Resiner, W. Tremel, Inorg. Chem. 36 (1997) 352–355.
[12] W.T.A. Harrison, M.L.F. Phillips, A.V. Chavez, T.M. Nenoff, J. Mater. Chem. 9 (1999) 3087–3092.
[13] S. Ekambaram, S.C. Sevov, Inorg. Chem. 39 (2000) 2405–2410.
[14] (a) B. Bazán, J.L. Mesa, J.L. Pizarro, L. Lezama, M.I. Arriortua, T. Rojo, Inorg. Chem. 39 (2000) 6056–6060;
(b) B. Bazán, J.L. Mesa, J.L. Pizarro, A. Goñi, L. Lezama, M.I. Arriortua, T. Rojo, Inorg. Chem. 40 (2001) 5691–5694;
(c) B. Bazán, J.L. Mesa, J.L. Pizarro, M.I. Arriortua, T. Rojo, Mater. Res. Bull. 38 (2003) 1193–1202;
(d) B. Bazán, J.L. Mesa, J.L. Pizarro, L. Lezama, J.S. Garitaonandia, M.I. Arriortua, T. Rojo, Solid State Sci. 5 (2003) 1291–1301;
(e) B. Bazán, J.L. Mesa, J.L. Pizarro, A. Peña, M.I. Arriortua, T. Rojo, Z. Anorg. Allg. Chem. 631 (2005) 2026–2032;
(f) B. Bazán, J.L. Mesa, J.L. Pizarro, L. Lezama, A. Peña, M.I. Arriortua, T. Rojo, J. Solid State Chem. 179 (2006) 1459–1468.
[15] S. Chakrabarti, S. Natarajan, Angew. Chem., Int. Ed. 11 (2002) 1224–1226.
[16] (a) J.L. Guth, H. Keesler, R. Wey, Stud. Surf. Sci. Catal. 28 (1986) 121–128;
(b) G. Férey, J. Fluorine Chem. 72 (1995) 187–193;
(c) G. Ferey, T. Loiseau, D. Riou, In Advanced Inorganic Fluorides: Synthesis, in: T. Nakajima, B. Zemva, A. Tressaud (Eds.), Characterization and Applications, Elsevier Science, New York, 2000 Chapter 7;
(d) G. Férey, Chem. Mater. 13 (2001) 3084–3098.
[17] M. Estermann, L.B. McCusker, C. Baerlocher, A. Merrouche, H. Kessler, Nature 352 (1991) 320–323.
[18] T. Loiseau, G. Ferey, J. Solid State Chem. 111 (1994) 403–415.
[19] C. Sassoye, T. Loisseau, F. Taulelle, G. Ferey, Chem. Commun. (2000) 943–944.
[20] C. Sassoye, J. Marrot, T. Loisseau, G. Ferey, Chem. Mater. 14 (2002) 1340–1347.
[21] N. Guillou, Q. Gao, P.M. Forster, J.-S. Chang, M. Nogues, S.-E. Park, G. Ferey, A.K. Cheetham, Angew. Chem., Int. Ed. 40 (2001) 2831–2834.
[22] (a) S. Fernández, J.L. Mesa, J.L. Pizarro, L. Lezama, M.I. Arriortua, R. Olazcuaga, T. Rojo, Chem. Mater. 12 (2000) 2092–2098;
(b) M. Cavellec, D. Riou, J.M. Greneche, G. Ferey, Inorg. Chem. 36 (1977) 2187–2190;
(c) S.-H. Luo, Y.-C. Jiang, S.-L. Wang, H.-M. Kao, K.-H. Lii, Inorg. Chem. 40 (2001) 5381–5384;
(d) E.P. Zhang, Y. Wang, G. Zhu, Z. Shi, Y. Liu, H. Yuan, W. Pang, J. Solid State Chem. 154 (2000) 368–374.
[23] B. Bazán, J.L. Mesa, J.L. Pizarro, J. Rodríguez-Fernández, J. Sánchez-Marcos, A. Roig, E. Molins, M.I. Arriortua, T. Rojo, Chem. Mater. 16 (2004) 5249–5259.
[24] T. Loisseau, Y. Calage, P. Lacorre, G. Ferey, J. Solid State Chem. 111 (1994) 390–396.
[25] M.E. Hagerman, K.R. Poeppelmeier, Chem. Mater. 7 (1995) 602–621.
[26] CRYSALIS, version 171.32.5; Oxford Diffraction Ltd.: Oxford (2007).
[27] G.M. Sheldrick, SHELX97—Programs for Crystal Structure Analysis (Release 97-2), Institüt für Anorganische Chemie der Universität, Göttingen, Germany, 1998.
[28] E. Dowty, A. ATOMS, Computer Program for Displaying Atomic Structures, Shape Software, 521 Hidden Valley Road, Kingsport, TN, 1993.
[29] R.A. Brand, J. Lauer, D.M. Heralch, J. Phys. F: Met. Phys. 13 (1983) 675–683.
[30] P.I. Tordjman, R. Masse, J.C. Guitel, Z. Kristallogr. 139 (1974) 103–115.
[31] S. Alvarez, D. Avnir, M. Lunell, M. Pinsky, New J. Chem. 26 (2002) 996–1009.
[32] (a) ICDD (2010) Powder Diffraction File, PDF2-Inorganic and Organic PDF 01-082-1124;
(b) PDF 01-083-1554;
(c) PDF 01-070-2309;
(d) PDF 00-049-1087;
(e) PDF 01-082-2047;
(f) PDF 01-072-1538.
[33] K. Nakamoto, Infrared and Raman Spectra of Inorganic and Coordination Compounds, Wiley, New York, 1997.
[34] A.B.P. Lever, Inorganic Electronic Spectroscopy, Elsevier, Amsterdam, 1984.
[35] Y. Tanabe, S. Sugano, J. Phys. Soc. Jpn. 9 (1954) 753–766.
[36] (a) H.W. Wijn, L.R. Walker, J.L. Davis, H. Guggenheim, J. Solid State Commun. 11 (1972) 803–805;
(b) P.M. Richards, M.B. Salamon, Phys. Rev. B 9 (1974) 32–45;
(c) A. Escuer, R. Vicente, M.A.S. Goher, F.A. Mautner, Inorg. Chem. 34 (1995) 5707–5708;
(d) T.T.P. Cheung, Z.G. Soos, R.E. Dietz, F.R. Merritt, Phys. Rev. B 17 (1978) 1266–1276.
[37] R.L. Carlin, Magnetochemistry, Springer-Verlag, Berlin, 1986.